Journal of Food Biochemistry

WILEY

RESEARCH ARTICLE OPEN ACCESS

Polysaccharide From *Ficus pumila* Alleviates Acute Lung Injury in Mice Through Regulating MAPK/NF-κB Pathway and Gut Microbiota

Shiying Mai[1] | Liyan Li[2] | Yinfeng Tan[2] | Minghai Fu[2] | Junqing Zhang[2] | Fang Zhang[2] | Yonghui Li[2] | Qi Wang[1] | Yuhuang Wu[1,2]

[1]Key Laboratory of Emergency and Trauma of Minis Try of Education, Key Laboratory of Hainan Trauma and Disast er Rescue, Department of Pharmacy, The First Affiliated Hospital, Hainan Medical University, Haikou, Hainan 570102, China | [2]Key Laboratory of Tropical Translational Medicine of Ministry of Education, Hainan Provincial Key Lab of R&D on Tropic Herbs, School of Pharmacy, Hainan Medical University, Haikou, Hainan 571199, China

Correspondence: Qi Wang (lizzywangqi@163.com) | Yuhuang Wu (1324353945@qq.com)

Received: 29 September 2024 | **Revised:** 10 January 2026 | **Accepted:** 27 January 2026

Academic Editor: Hongxun Tao

Keywords: acute lung injury | *Ficus pumila* | gut microbiota | polysaccharide | structural characterization

ABSTRACT

Background: Lihuabidouyan Tablet is a compound Chinese herb preparation used for the treatment of respiratory diseases. As the main active ingredient in it, *Ficus pumila* (*F. pumila*) contains polysaccharides that exert unique biological activity. In this study, polysaccharides in *F. pumila* were extracted and purified, and the protective effect and mechanism of action of *F. pumila* polysaccharide 1-1 (FPP1-1) in lipopolysaccharide (LPS)-induced acute lung injury (ALI) mice were discussed.

Methods: BALB/c mice were randomly divided into control, model, dexamethasone (DEX), and FPP-1-1 groups (50, 100, and 200 mg/kg), and the drug was administered by gavage for one week. Hematoxylin–eosin staining (H&E) and wet/dry ratio were used to evaluate lung injury and pulmonary edema. The ELISA was used to detect inflammatory factors. qRT-PCR was used to examine mRNA expression in tissues. Proteins related to inflammation were evaluated by western blotting. 16S rDNA sequencing was used to analyze the gut microbiota.

Results: FPP-1-1 significantly reduced lung injury in the ALI mice and significantly reduced levels of the proinflammatory factors interleukin (IL)-6 and tumor necrosis (TNF)-α and promoted the anti-inflammatory factor IL-10 in bronchoalveolar lavage fluid. FPP-1-1 inhibited the expression of phospho-ERK1/2, phospho-P38, and phospho-NF-κB p65 proteins. FPP-1-1 also increased the diversity of the gut microbiota and increased the abundance of *Lachnospiraceae* in the ALI mice. Correlation analysis results showed that there was a significant correlation between the MAPK/NF-κB pathway and inflammatory cytokines and gut microbiota in ALI mice.

Conclusion: The present study characterized the structure and molecular weight of a novel homogeneous polysaccharide, FPP-1-1, isolated from *F. pumila*. In addition, FPP-1-1 affected the expression of inflammatory factors by inhibiting the MAPK/NF-κB pathway. FPP-1-1 also restored the diversity of gut microbiota and changed the relative abundance of key bacterial genera such as *Lachnospiraceae* and *Alloprevotella*, suggesting that the "gut–lung" axis may serve as a crucial pathway through which FPP-1-1 exerts its effect.

Shiying Mai and Liyan Li these authors contributed equally to this work and share first authorship.

This is an open access article under the terms of the Creative Commons Attribution License, which permits use, distribution and reproduction in any medium, provided the original work is properly cited.

Copyright © 2026 Shiying Mai et al. *Journal of Food Biochemistry* published by John Wiley & Sons Ltd.

1 | Introduction

Acute lung injury (ALI) is one severe pulmonary disease accompanied by respiratory distress, pulmonary infiltration, severe alveolar edema, and progressive hypoxemia [1, 2]. It is a common cause of death in clinical patients with respiratory diseases. Systemic inflammatory response and excessive inflammatory factors accumulated in the lung tissue are the main causes of pulmonary interstitial edema [3]. Currently, the main methods used to treat ALI are to improve ventilatory and drug treatments. Glucocorticoids are commonly used in drug therapy [4], but morbidity and mortality rates are still as high as 30%–40% [5].

The influence of gut microbiota on lung immunity is known as the "gut–lung" axis, through which intestinal microflora can regulate lung disease [6]. Gut microbiota dysbiosis may compromise the intestinal barrier, triggering the immune system, allowing harmful microorganisms to enter the lungs, and aggravating lung tissue damage. Restoring the balance of gut microbiota has become an important means to treat lung diseases.

Ficus pumila (*F. pumila*) is an evergreen climbing or creeping plant of the genus *Ficus*, which is mainly distributed in Southern China and Japan. As a functional food, pectin and various fatty acids derived from *F. pumila* have been utilized in the food industry. The fruit of *F. pumila* is processed into a mucilage extract through kneading and squeezing with water in China. This mucilage extract forms a gel known as "Liangfen" at room temperature, which has long been regarded as alleviating summer heat and promoting digestion, and is marketed as a functional food [7, 8]. Furthermore, *F. pumila* tea prepared from the leaves of *F. pumila* can lower blood pressure and improve dyslipidemia in individuals with hypertension, dyslipidemia, liver dysfunction, and gout [9]. The root, fruit, and leaves of *F. pumila* have also been used for hemostasis, reducing swelling, clearing heat, and detoxifying. Previous studies reported that the methanolic extract of *F. pumila* possesses anti-inflammatory and analgesic activities [10].

Polysaccharides are abundant natural polymers that are mostly derived from plants or animals [11]. They have attracted increasing attention owing to their excellent anti-inflammatory [12], antitumor [13], immunomodulatory [14], antioxidant [15], antiviral [16], and other biological activities. *F. pumila* polysaccharides were not cytotoxic and stimulated NO production, production of the proinflammatory cytokines, and phagocytic activity [7]. As an inflammation-related disease, *F. pumila* polysaccharides may have a beneficial effect on lung injury. However, the ALI protective activity of *F. pumila* polysaccharides has not yet been reported.

In this study, a polysaccharide named *F. pumila* polysaccharide 1-1 (FPP1-1) was isolated from *F. pumila,* and its structure was detected. Further investigated the protective effect of FPP-1-1 on ALI and its effect on the MAPK/NF-κB pathway. In addition, the effect of FPP-1-1 on gut microbiota was evaluated through 16S rDNA sequencing, aiming to elucidate the mechanism of FPP-1-1 from the perspective of gut microbiota.

2 | Materials and Methods

2.1 | Materials

Fresh aerial portions of *F. pumila* were collected from Yongxing town in the Hainan Province, China. Whatman supplied DEAE-52 cellulose (UK). Sephadex G-100 was obtained from Cytiva (USA). The China Institute of Food and Drug Control provided dextran standards. Aladdin (China) provided trifluoroacetic acid (TFA) and 1-phenyl-3-methyl-5-pyrazolone (PMP). Monosaccharide standards were obtained from Sinopharm Chemical Reagent Co. Ltd. (China). The Congo red reagent was purchased from Aladdin Reagent Co., Ltd. (China). The reagents used for the high-performance liquid chromatography (HPLC; RID-20, SHIMADZU, Japan) analysis were of chromatography grade. All other reagents used were of analytical grade.

2.2 | Preparation of Polysaccharides

The aerial parts of fresh *F. pumila* L. (10 kg) were extracted three times with hot water (1:10, w/v), each extraction lasting 2 h. The three extracts were combined, and then concentrated to 1/25 of the initial volume, followed by the addition of four volumes of 95% ethanol. The sample was then stored at 4°C for 24 h, and the precipitate was collected by centrifugation. The precipitates were dissolved in water, 95% ethanol was added again, and the sample was precipitated three times. After centrifugation, the supernatant was discarded, and the precipitate was dried at 60°C under reduced pressure to obtain dried extracts. Ten grams of dried extract was dissolved in 1000 mL of water, stirred for 3 h, and centrifuged (4000 rpm, 10 min). The supernatant was freeze-dried to obtain a crude polysaccharide named FPP.

Twenty milliliters of distilled water was added to dissolve 400 mg of FPP and centrifuged (4000 rpm, 10 min). The supernatant was loaded onto a DEAE-52 column (2.6 × 30 cm) and eluted sequentially with purified water, 0.1 mol/L NaCl, 0.2 mol/L NaCl, and 0.4 mol/L NaCl as mobile phases at a flow rate of 1.0 mL/min. Each mobile phase was eluted for 10 min, yielding four independent elution fractions corresponding to the respective phases, which were designated as FPP-0, FPP-1, FPP-2, and FPP-3. The major fraction (FPP-1) was added to a Sephadex G-100 column (2.6 × 50 cm) with distilled water as the mobile phase. The eluate containing polysaccharide was collected from the tube, and one purified polysaccharide, named FPP-1-1, was obtained by freeze-drying.

2.3 | Analysis of FPP-1-1 Components

The total polysaccharide content of the purified polysaccharide was determined by the phenol-sulfuric acid method using D-anhydrous glucose (Acros Organics, USA) as the standard. Quantification of the protein content of FPP-1-1 was done using the Bradford method [17]. The uronic acid content in FPP-1-1 was determined using the *m*-hydroxydiphenyl method [18], with galacturonic acid (Wako, Japan) serving as the standard. The absorbance was measured at 526 nm using a UV–Vis spectrophotometer (V-650, JASCO, Japan).

2.4 | Measurement of the Molecular Weight (Mw)

FPP-1-1 Mw is detected through performing high-performance gel permeation chromatography (HPGPC; RID-20A, Shimadzu, Kyoto, Japan). FPP-1-1 was analyzed using a TSK gel G-4000 PWxL (7.8 mm × 30 cm, Tosoh Biosep, Japan) at a column temperature of 30°C. Dextran (Merck, Germany) standards (Mw ranges 13050–2000000 Da) were prepared at a concentration of 1 mg/mL, and the standard curve was plotted. A concentration (1 mg/mL) of FPP-1-1 was prepared, and the Mw of FPP-1-1 was computed from the standard curve [19].

2.5 | FPP-1-1 Monosaccharide Composition

Ten milligrams of FPP-1-1 are dissolved in 2 mL of 4 mol/L TFA and hydrolyzed for 4 h at 110°C. The hydrolysate was mixed with methanol and rotated at 60°C, which completely removed the TFA, and the hydrolysate has been dissolved in 0.5 mL of distilled water. Next, 0.2 mL of 0.5 mol/L PMP solution and 0.1 mL of 0.6 mol/L NaOH were added and reacted for 70 min at 70°C. The solution was neutralized with 0.2 mL of 0.3 mol/L muriatic acid and washed with a small amount of dichloromethane. The same derivatization procedure was performed on the standard monosaccharide mixtures (Man, Rib, Rha, GlcUA, GalUA, Glc, Gal, Ara, and Fuc). The standard solutions and prepared samples were detected using an HPLC system equipped with a C18 column (4.6 × 150 mm). The analytical conditions were as follows: flow rate, 1.0 mL/min; mobile phase, 100% acetonitrile (A): phosphate-buffered salt solution (B, pH 6.7) = 17.5:82.5; and detection wavelength, 254 nm [20].

2.6 | Analysis of the Ultraviolet Spectrum

FPP-1-1 was dissolved in water and prepared as a 1 mg/mL sample, scanned using a UV–Vis spectrophotometer in the range of 200–600 nm.

2.7 | Fourier Transform Infrared (FTIR) Spectroscopy Analysis

Two milligrams of FPP-1-1 mixed with 200 mg of potassium bromide (Shanghai Aladdin Bio-Chem Technology Co., LTD, China) was pressed into transparent slices using a cylindrical mold, and the spectra were recorded and analyzed using FTIR (Frontier LR 64912C, Perkin-Elmer, USA) spectroscopy.

2.8 | Congo Red Analysis

The conformation of the FPP-1-1 structure was determined using the Congo red assay [21, 22]. The FPP-1-1 sample (1 mg/mL) was blended completely with Congo red solution (100 μmol/L; Shanghai Aladdin Bio-Chem Technology Co., LTD, China) in a 1:1 (v/v) ratio. Various volumes of NaOH (1 mol/L) were added to the mixture to obtain a series of NaOH concentrations (0.1, 0.2, 0.3, 0.4, 0.5 mol/L). After standing for 10 min, the samples were subjected to full-wavelength scanning using a UV–Vis spectrophotometer to determine the maximum absorption wavelength. The concentration of NaOH in the solution was used as the abscissa, and the maximum absorption wavelength was plotted as the ordinate in the graph.

2.9 | Evaluation of the Anti-Inflammatory Effect of FPP-1-1 In Vivo

2.9.1 | Animals and Treatment

Seventy-two male BALB/c mice (22–24 g, 4–8 weeks old) were kept in an environment with humidity of 55 ± 5%, a temperature of 22 ± 2°C, and a brightness cycle of 12 h for one week. Mice were randomly selected into six groups of 12 mice each: control, model, dexamethasone (DEX), and FPP-1-1 groups. The control group was administered physiological saline for 7 d; the model group was administered saline for 7 d, and 10 mg/kg lipopolysaccharide (LPS) was injected intraperitoneally for 2 h after the last gavage to establish the ALI model; the DEX group was first administered saline for 6 d, followed by an intraperitoneal injection of 5 mg/kg DEX on the last day, and 10 mg/kg LPS was injected intraperitoneally 2 h later; FPP-1-1 (50 mg/kg, 100 mg/kg, 200 mg/kg) was administered by gavage for 7 d, and 10 mg/kg LPS was injected intraperitoneally 2 h after the last dose. Within 12 h of intraperitoneal injection of LPS, mouse lung tissue, lung bronchoalveolar lavage fluid (BALF), and gut contents were collected for subsequent analysis.

This study was performed in accordance with Experimental Animal Administration regulations issued by the State Committee of Science and Technology of the People's Republic of China. All animal experiments were approved in advance by the Institutional Animal Care and Use Committee of Hainan Medical University (Approval No. NM-LL-2021-06-15-1).

2.9.2 | Lung Wet/Dry (W/D) Ratio

Upper right lung lobes were collected to determine the W/D ratio. The tissues were rinsed with saline, blotted with absorbent paper to absorb surface water, and the wet weight was measured. All wet tissues were dried at 85°C for 48 h to acquire the dry weight. The resulting wet weight was divided by dry weight to obtain the W/D ratio.

2.9.3 | Hematoxylin–Eosin (H&E) Staining

The middle lobe of the right lung was selected for histological examination. Lung tissues were fixed and stored in 4% paraformaldehyde, followed by H&E staining to visualize the pathological changes in each group of lung tissues.

2.9.4 | Acquisition of BALF

After 12 h of intraperitoneal LPS injection, the mice were anesthetized, and the trachea was isolated. Subsequently, the whole lungs were lavaged with 1.5 mL of ice-chilled PBS, drawn out with a syringe after a one-minute duration to harvest BALF. Subsequently, the collected BALF is then centrifuged at 1500 rpm for 15 min at 4°C, and the supernatant is collected and stored at −80°C.

2.9.5 | ELISA

Following the kit instructions, the levels of interleukin (IL)-6, tumor necrosis (TNF)-α, and IL-10 in BALF were measured using

the corresponding ELISA kits (Sangon Biotechnology, Shanghai, PR China).

2.9.6 | Real-Time PCR Analysis

Total RNA was extracted from each lung tissue sample using the Eastep Super Total RNA Extraction Kit (Beijing Promega Biotech Co., Ltd., China), according to the manufacturer's instructions. RNA was measured quantitatively and qualitatively using a UV–Vis spectrophotometer. The obtained RNA samples were reverse transcribed into cDNAs using Hifair II 1st Strand cDNA Synthesis SuperMix for qPCR (gDNA digester plus, Yeasen Biotechnology Co., Ltd., China) according to the instructions of the kit. The obtained cDNAs were stored at −80°C. The extracted cDNAs were amplified using Hieff qPCR SYBR Green Master Mix (Low Rox Plus, Yeasen Biotechnology Co., Ltd., China) according to the instructions of the kit with a gradient fluorescence qRT-PCR instrument (CFX96 Touch, Bio-Rad Laboratories, USA). Three phases of amplification are carried out: a predenaturation cycle lasting 5 min at 95°C, 40 cycles of denaturation for 10 s at 95°C, annealing for 20 s at 58°C, and extension for 20 s at 72°C. A melting curve was generated to verify the specificity of the amplification products. The target genes included TNF-α, IL-6, and IL-10 (Sangon Biotech, China). GADPH (Sangon Biotech, China) was used as the internal reference gene, and the TBGreen and $2^{-\Delta\Delta Ct}$ methods were employed to determine mRNA expression levels. The sequences used in the present study are listed in Table 1.

2.9.7 | Western Blotting Analysis

Western blotting was used to analyze the protein levels in lung tissues. Lung tissues were homogenized on ice in RIPA lysis buffer containing PMSF and phosphatase inhibitors using a homogenizer. Lung tissue homogenates were incubated at 4°C for 30 min and centrifuged at 10,000 rpm for 15 min at 4°C. The protein concentrations in the supernatant were determined using a BCA assay kit. Each sample was separated electrophoretically on a 10% SDS–PAGE gel and transferred to a PVDF membrane. Membranes were blocked with 5% (w/v) skim milk in Tris-buffered saline containing 0.1% Tween-20 (TBST) for 1 h at room temperature. Subsequently, PVDF membranes were incubated with specific primary antibodies (p38, p-p38, ERK1/2, and *p*-ERK1/2 purchased from Abcam, UK; NF-κB p65 and p-NF-κB p65 purchased from Proteintech, USA) overnight at 4°C. The PVDF membranes were then washed, and horseradish peroxidase-conjugated secondary antibodies were added and incubated for 1 h. Protein bands were detected using an ECL chemiluminescence kit. GAPDH was used as an internal control. The analysis was performed using the Image Lab software (Chemi DocTM XRS+, Bio-Rad, USA).

TABLE 1 | Sequences for qRT-PCR.

Name	Sequence (5′ ⟶ 3′)	Length
GAPDH-F	TGTTTCCTCGTCCCGTAGA	19
GAPDH-R	ATCTCCACTTTGCCACTGC	19
TNF-α-F	CGCTCTTCTGTCTACTGAACTTCGG	25
TNF-α-R	GTGGTTTGTGAGTGTGAGGGTCTG	24
IL-6-F	CTTCTTGGGACTGATGCTGGTGAC	24
IL-6-R	TCTGTTGGGAGTGGTATCCTCTGTG	25
IL-10-F	TTCTTTCAAACAAAGGACCAGC	22
IL-10-R	GCAACCCAAGTAACCCTTAAAG	22

2.9.8 | High-Throughput Sequencing

In order to explore the effect of the FPP-1-1 on gut microbiota, the gut contents of mice in the medium-dose FPP-1-1 (100 mg/kg) group, which showed a significant beneficial effect, were selected for high-throughput sequencing. After the model was established, fresh feces were gathered on the 7th day. Bacterial genomic DNA was extracted using the E.Z.N.A. Soil DNA Kit (Omega Bio-Tek, USA). The highly variable region of prokaryotic 16S rDNA was amplified and classified. Next, the PCR products were analyzed by agarose gel electrophoresis, and the qualified products were mixed as required. MiSeq sequencing, OTU cluster analysis, and species taxonomy analysis were then performed. MiSeq control software (Majorbio, China) was used for the data analysis. Finally, Spearman correlation analysis was conducted using R Version 4.3.1 to evaluate the associations between gut microbiota and the MAPK, NF-κB, and cytokines.

2.10 | Statistical Analysis

All experiments were performed with three independent replicates. Data are expressed as mean ± standard deviation (SD). One-way analysis of variance (ANOVA) followed by Tukey's post hoc test was used for multiple comparisons among groups, as performed using GraphPad Prism 7 (GraphPad Software, USA). Spearman correlation analysis was performed using R Version 4.3.1. Differences were considered statistically significant at $p < 0.05$.

3 | Results

3.1 | Chemical Components of FPP-1-1

Polysaccharide purification using DEAE-52 and Sephadex G-100 columns yielded a single-peak fraction named FPP-1-1. The main chemical composition of FPP-1-1 is listed in Table 2. The total sugar content of FPP-1-1 was 98.4%, and the protein content of FPP-1-1 was 0.86%, which is consistent with the absorption of the UV–Vis spectra (Figure 1(a)). The uronic acid content was 25.14%.

3.2 | Mw and Monosaccharide Composition

The relative Mw of FPP-1-1 was determined using HPGPC based on the dextran standard curve, as shown in Figure 1(b). FPP-1-1 generated a single symmetric peak, signifying that FPP-1-1 is a homogeneous polysaccharide with a Mw of 1.29×10^6 Da. According to the HPLC chart of mixed standard monosaccharides, the FPP-1-1 monosaccharide composition was analyzed by HPLC, as shown in Figure 2. FPP-1-1 consists of Rha, Man, GlcUA, Glc, GalUA, Gal, Ara, and Fuc with the ratio of 5.55%: 1.79%: 1.05%: 3.67%: 1.00%: 49.52%: 13.43%: 1.10%.

TABLE 2 | The chemical composition of FPP-1-1

Carbohydrate	Protein	Uronic acid
98.4%	0.8%	25.14%

3.3 | FTIR Spectrum

A distinct peak for polysaccharides can be seen in Figure 1(c) at a powerful and wide peak at 3395.98 cm^{-1}, which reflects the O-H stretching vibration [23]. The presence of the aldehyde group was revealed through the stretching vibration of the C-H bond at 2950-3000 cm^{-1} and the stretching vibration of the -CHO and C-O bonds at 1633.49 cm^{-1} [24]. Strong absorption peaks due to C-O stretching vibrations of pyranose are exhibited in the range of 1104.65 cm^{-1} and 988.79 cm^{-1} [25]. The presence of an absorption peak at 859.1 cm^{-1} may indicate the presence of an α-glucopyranoside structure, which also indicates the presence of the uronic acid structure in FPP-1-1 [22, 26].

3.4 | Congo Red Analysis

A Congo red complex was created as a result of the interaction between triple-helical polysaccharides and Congo red dye. Over a range of concentrations, the maximum absorption wavelength of the Congo red complex shifts toward a bathochromic shift and gradually reaches a plateau [27, 28]. The maximum absorption wavelength of the combination of FPP-1-1 and Congo red in NaOH solution remained unaltered when compared to that of the Congo red blank group, according to the experimental results (Figure 1(d)). In aqueous solution, the data revealed that FPP-1-1 does not have a triple-helix structure.

3.5 | Evaluation of the Protective Effect of FPP-1-1 on ALI In Vivo

3.5.1 | Effects of FPP-1-1 on LPS-Induced ALI in Mice

H&E-stained sections were used to assess the histopathological pattern and extent of lung damage in mice. The alveolar structure of the control group (Figure 3(a)) was intact, the alveolar lumen was visible, exudate was not obvious, and no histopathological changes were observed. The alveoli in the model group are shown in Figure 3(b). LPS caused alveolar hemorrhage and collapse, neutrophil infiltration in the space or blood vessel wall, and thickening of the alveolar septum in mice. The results in Figures 3(c), 3(d), 3(e), and 3(f) show that FPP-1-1 treatment significantly attenuated LPS-induced histopathological changes in the mouse lungs, and the 100 mg/kg FPP-1-1 had the most beneficial effect.

To determine the severity of the pulmonary edema, we estimated the lung W/D ratio (Figure 3(g)). In comparison to the control group, the W/D ratio was significantly higher in the model group ($p < 0.01$). The W/D ratio was much lower than that of the model group following treatment with FPP-1-1 (50 mg/kg, $p < 0.001$; 100 mg/kg, $p < 0.001$), and the beneficial effect of 100 mg/kg FPP-1-1 was the most significant.

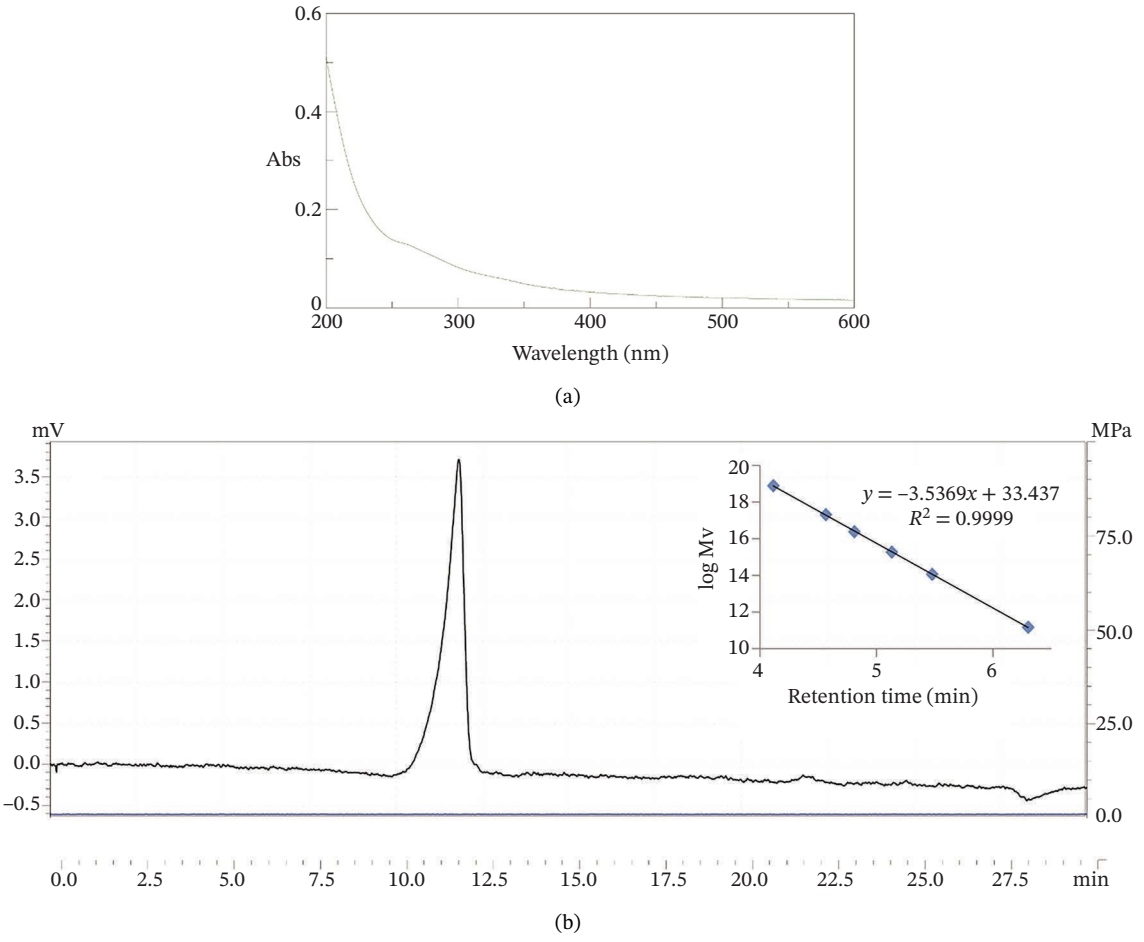

FIGURE 1 | (Continued)

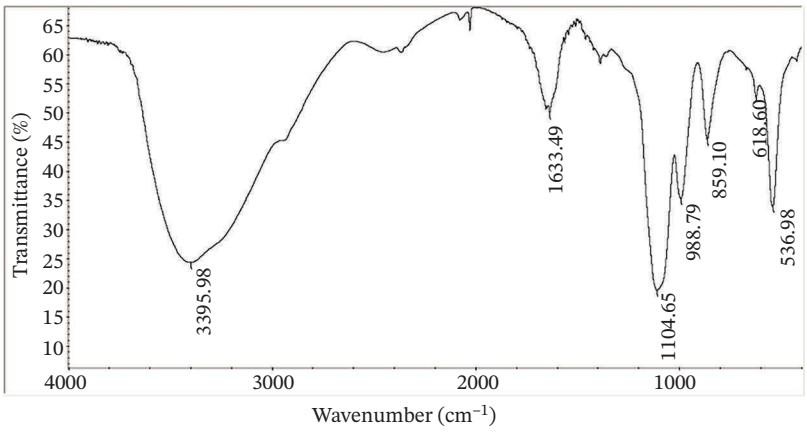

(c)

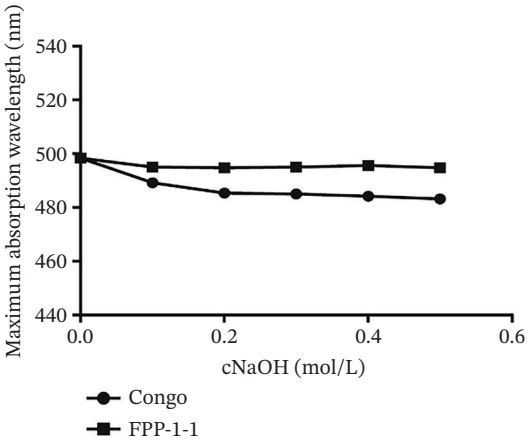

(d)

FIGURE 1 | FPP-1-1 UV–Vis full wavelength spectrum (a). HPGPC chromatograph of FPP-1-1 (b). FT-IR spectrum of FPP-1-1 (c). The maximum absorption of Congo red and FPP-1-1 in the presence of various concentrations of NaOH (d).

3.5.2 | FPP-1-1 Inhibits the Expression of Inflammatory Cytokines in the BALF

The levels of inflammatory factors in BALF are shown in Figure 4. LPS induction significantly improved the TNF-α ($p < 0.001$), IL-6 ($p < 0.01$), and reduced the IL-10 ($p < 0.01$) compared to the control group. Compared to the model group, TNF-α expression was considerably reduced in the FPP-1-1 groups (50 mg/kg, $p < 0.01$; 100 mg/kg, $p < 0.01$), IL-6 expression was significantly lower in the FPP-1-1 groups (50 mg/kg, $p < 0.001$; 100 mg/kg, $p < 0.01$; 200 mg/kg, $p < 0.01$), and IL-10 expression was higher in the FPP-1-1 group (100 mg/kg, $p < 0.05$; 200 mg/kg, $p < 0.05$). In summary, FPP-1-1 effectively inhibited

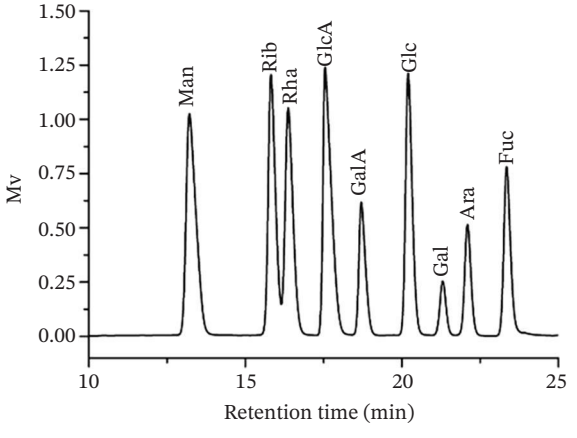

(a)

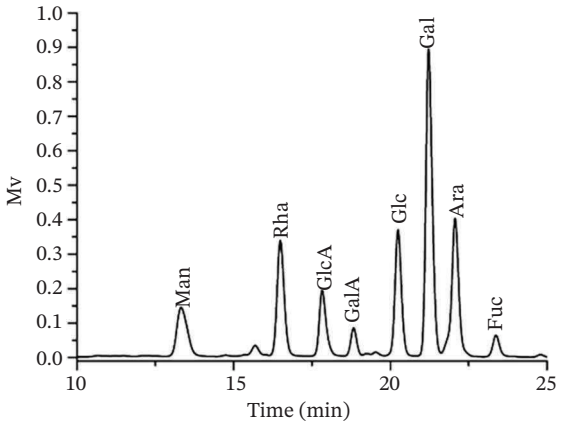

(b)

FIGURE 2 | Analysis of the monosaccharide composition of FPP-1-1. Standard monosaccharides (a) and FPP-1-1 (b).

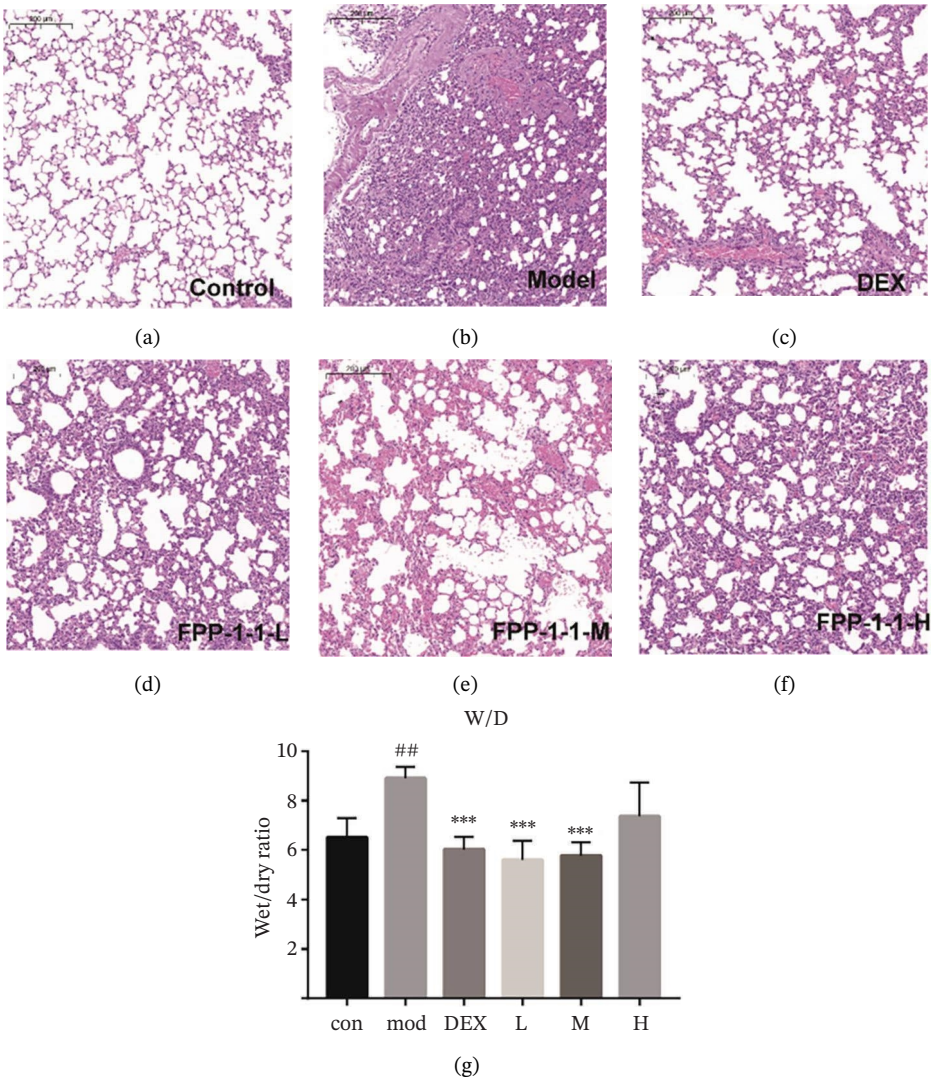

FIGURE 3 | FPP-1-1 improves lung tissue injury in mice ($n = 6$). Hematoxylin–eosin staining of mice lung tissue (a–f); lung W/D weight ratio (g). $L = 50$ mg/kg, $M = 100$ mg/kg, H = 200 mg/kg. $^{\#\#}p < 0.01$ contrasted with control group; $^{***}p < 0.001$ contrasted with model group.

the release of proinflammatory factors IL-6 and TNF-α and promoted the release of anti-inflammatory factor IL-10 in mice to improve lung inflammation.

3.5.3 | Effect of FPP-1-1 on Cytokine mRNA Expression Levels in ALI Mice

The effects of FPP-1-1 on the mRNA expression of TNF-α, IL-6, and IL-10 in ALI mouse lung tissues were examined by qRT-PCR. The results are shown in Figure 5. In contrast to the control, TNF-α ($p < 0.01$) and IL-6 ($p < 0.01$) mRNA expression levels were considerably increased in the model group. In contrast to the model group, the TNF-α (all doses, $p < 0.01$) and IL-6 (all doses, $p < 0.01$) mRNA expression levels were significantly downregulated by the FPP-1-1 treatments, and the mRNA levels of IL-10 were significantly increased by the FPP-1-1 treatments (50 mg/kg, $p < 0.01$; 100 mg/kg, $p < 0.05$; 200 mg/kg, $p < 0.01$). The results were consistent with those of ELISA; FPP-1-1 effectively decreased the mRNA expression of the inflammatory factors TNF-α and IL-6 while increasing IL-10 mRNA expression.

3.5.4 | Effects of FPP-1-1 on Levels of Proteins in the MAPK Pathway in ALI Mice

In the present study, western blotting was used to measure the levels of proteins related to the MAPK signaling pathway, namely p38/p-p38 and ERK1/2/p-ERK1/2 proteins, and phosphorylation levels were calculated as p-ERK1/2/ERK1/2 and p-p38/p38 ratios. As shown in Figure 6, following LPS stimulation, the p-ERK1/2/ERK1/2 ($p < 0.001$) and p-p38/P38 protein levels were considerably increased. After treatment with FPP-1-1, the levels of *p*-ERK1/2/ERK1/2 (100 mg/kg, $p < 0.05$; 200 mg/kg, $p < 0.01$) and p-p38/P38 (100 mg/kg, $p < 0.05$; 200 mg/kg, $p < 0.01$) proteins were considerably reduced.

3.5.5 | Effect of FPP-1-1 on the Levels of Proteins in the NF-κB Pathway in ALI Mice

The levels of NF-κB p65/p-p65 proteins in this signaling pathway were detected using western blotting, and the phosphorylation level was calculated as the NF-κB p-p65/p65 ratio. As shown in Figure 6, the level of NF-κB p-p65/p65 increased in the model

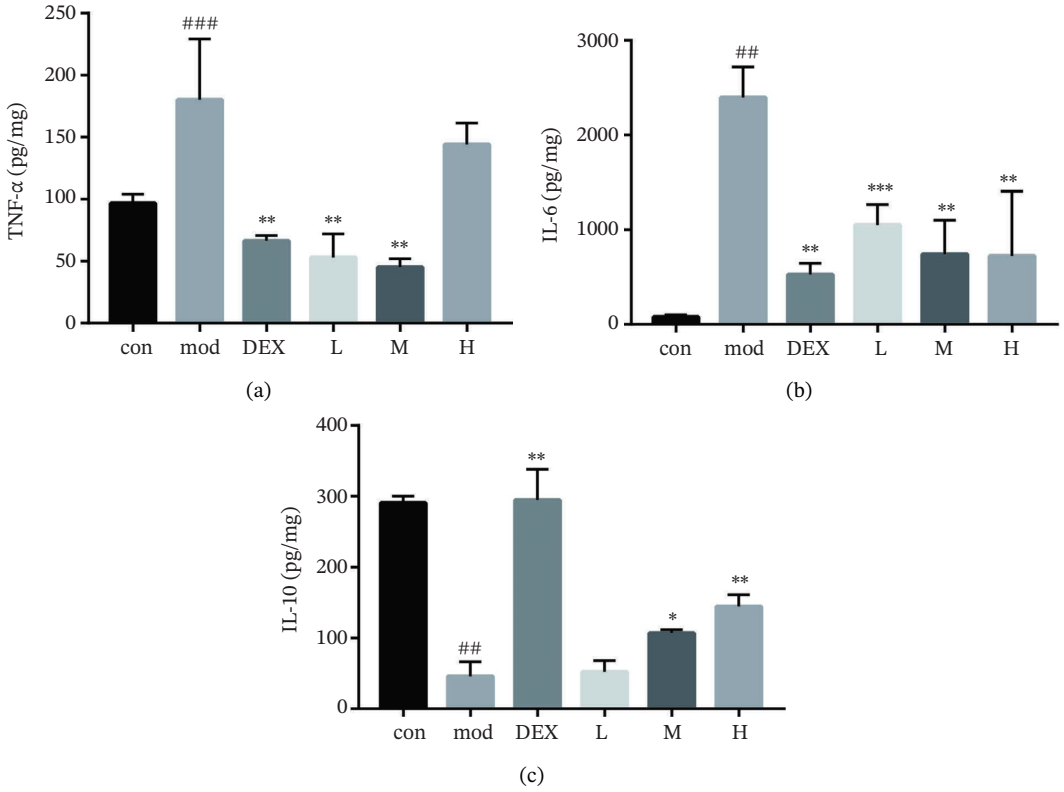

FIGURE 4 | FPP-1-1 effectively inhibited the IL-6 and TNF-α and promoted the IL-10 in bronchoalveolar lavage fluid ($n = 6$). The levels of TNF-α (a), IL-6 (b), and IL-10 (c) in the BALF. $L = 50$ mg/kg, $M = 100$ mg/kg, H = 200 mg/kg. $^{\#\#\#}p < 0.001$ contrasted with control group; $^{*}p < 0.05$ and $^{**}p < 0.01$ contrasted with model group.

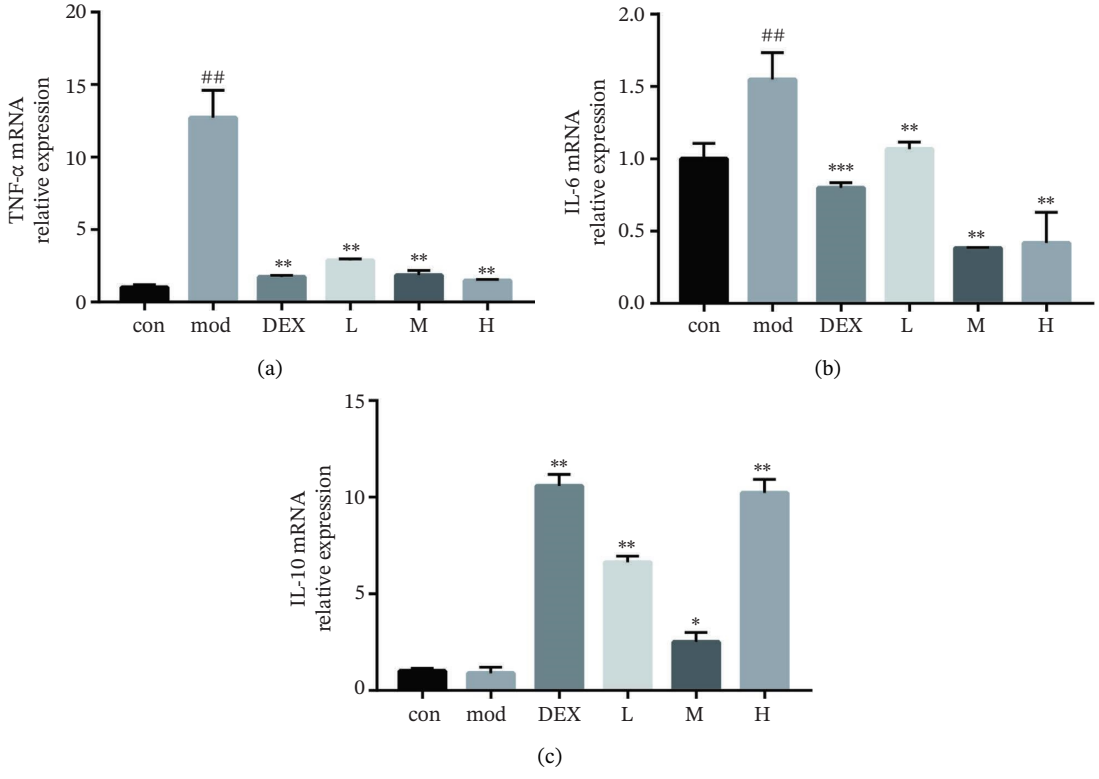

FIGURE 5 | FPP-1-1 effectively inhibited the mRNA of IL-6 and TNF-α and promoted the mRNA of IL-10 in the lung ($n = 6$). The mRNA levels of TNF-α (a), IL-6 (b), and IL-10 (c) in the lung. $L = 50$ mg/kg, $M = 100$ mg/kg, H = 200 mg/kg. $^{\#\#}p < 0.01$ contrasted with control group; $^{*}p < 0.05$ and $^{**}p < 0.01$ contrasted with model group.

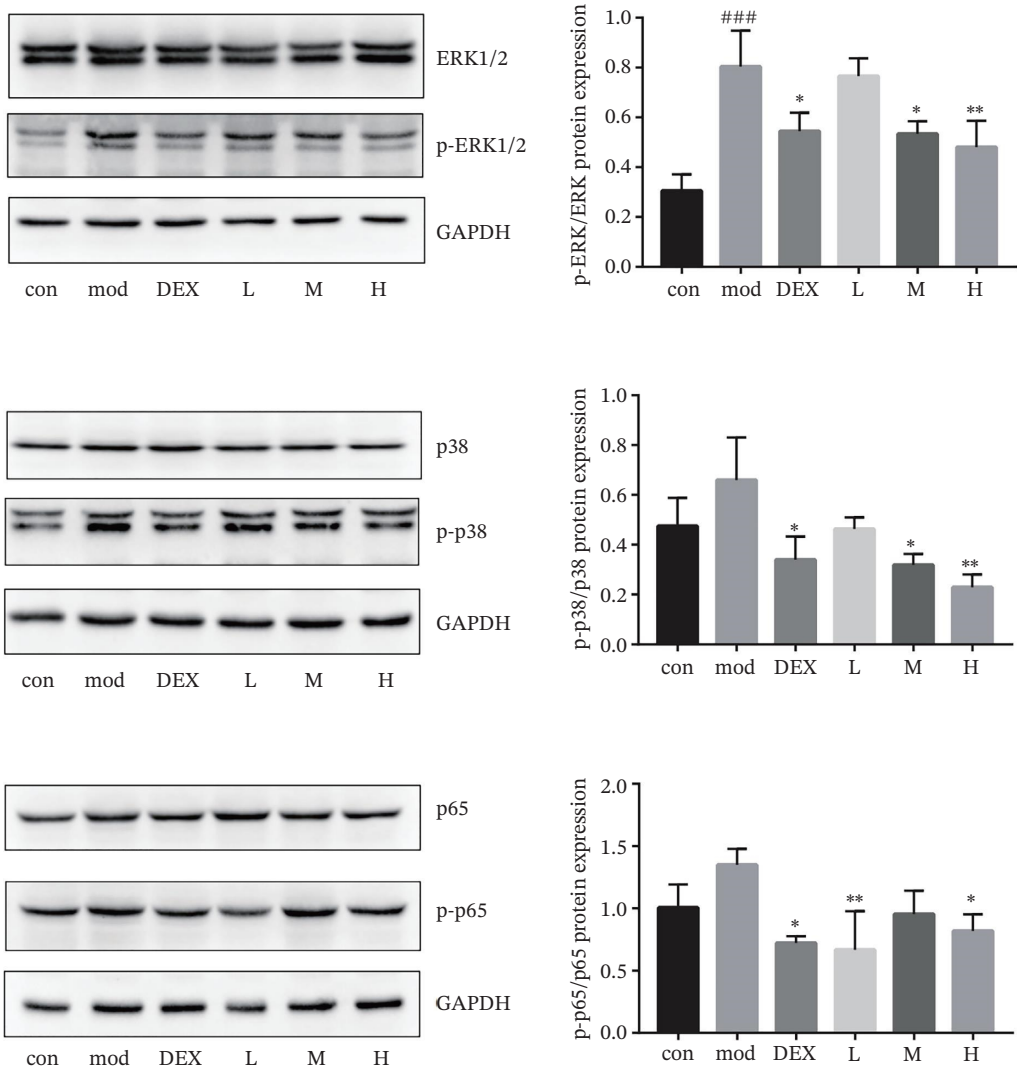

FIGURE 6 | FPP-1-1 inhibiting the activity of the NF-κB and MAPK pathways ($n = 6$). Effect of FPP-1-1 on the levels of proteins in the MAPK and NF-κB pathways in the lung. The levels of MAPK *p*-ERK1/2 (a), p-p38 (b), and NF-κB p-p65 (c). $L = 50$ mg/kg, $M = 100$ mg/kg, H = 200 mg/kg. $^{###}p < 0.01$ compared with the control group; $^{*}p < 0.05$ and $^{**}p < 0.01$ compared with the model group.

group after LPS stimulation (but the difference was not significant), whereas the level of NF-κB p-p65/p65 significantly decreased in the FPP-1-1 group (50 mg/kg, $p < 0.01$; 200 mg/kg, $p < 0.05$).

3.5.6 | Effects of FPP-1-1 on the Gut Microbiota

Considering that polysaccharides are a macromolecular drug, it is more likely that FPP-1-1 exerts its efficacy through the "gut–lung" axis. 16S rDNA gene sequencing showed that Bacteroidota, Firmicutes, and Proteobacteria were dominant in feces. We used principal co-ordinate analysis (PCoA) and principal ordinate analysis (PCA) to calculate the beta diversity index on the OTU level (Figure 7). The results revealed that the microbiota communities in the control group were far from the model group; the microbial community in the 100 mg/kg FPP-1-1 group was more similar to that in the control group. Compared with the control group, LPS injection altered the community structure of mice gut microbiota at phyla and genus levels, which mainly showed a decrease in the number of Firmicutes and an increase in the abundance of Bacteroides and Proteobacteria. Nevertheless, the abundance of Firmicutes increased, and the abundance of Bacteroidota and Proteobacteria decreased after 100 mg/kg FPP-1-1 treatment (Figure 8). The composition of gut microbiota at the genus level was further analyzed; by comparison with the control group, the abundance of *Lactobacillus* ($p < 0.01$), *Lachnoclostridium* ($p < 0.01$) and *Prevotellaceae_UCG-001* of the model group had a lower ($p < 0.05$), but a higher abundance of *norrank_f_Muribaculaceae* ($p < 0.01$), *Dubosiella* ($p < 0.01$), *Helicobacter*, *norrank_f_Oscillosporaceae* ($p < 0.05$), *norrank_f_norrank_o_Clostridia_UCG-014* ($p < 0.01$) in the model group. Treatment with 100 mg/kg FPP-1-1 reduced the abundance of *norrank_f_Muribaculaceae* ($p < 0.01$), *Dubosiella* ($p < 0.01$), *Helicobacter* ($p < 0.05$), *norrank_f_Oscillosporaceae* ($p < 0.01$), *norrank_f_norrank_o_Clostridia_UCG-014* ($p < 0.05$) and improved the abundance of *Lactobacillus* ($p < 0.05$), *Lachnoclostridium* ($p < 0.01$) and *Prevotellaceae_UCG-001* ($p < 0.01$) compared with the model group (Figure 9). These results suggest that 100 mg/kg FPP-1-1 treatment increases gut microbiota diversity and modulates the microbial community structure in the mice with LPS-induced ALI.

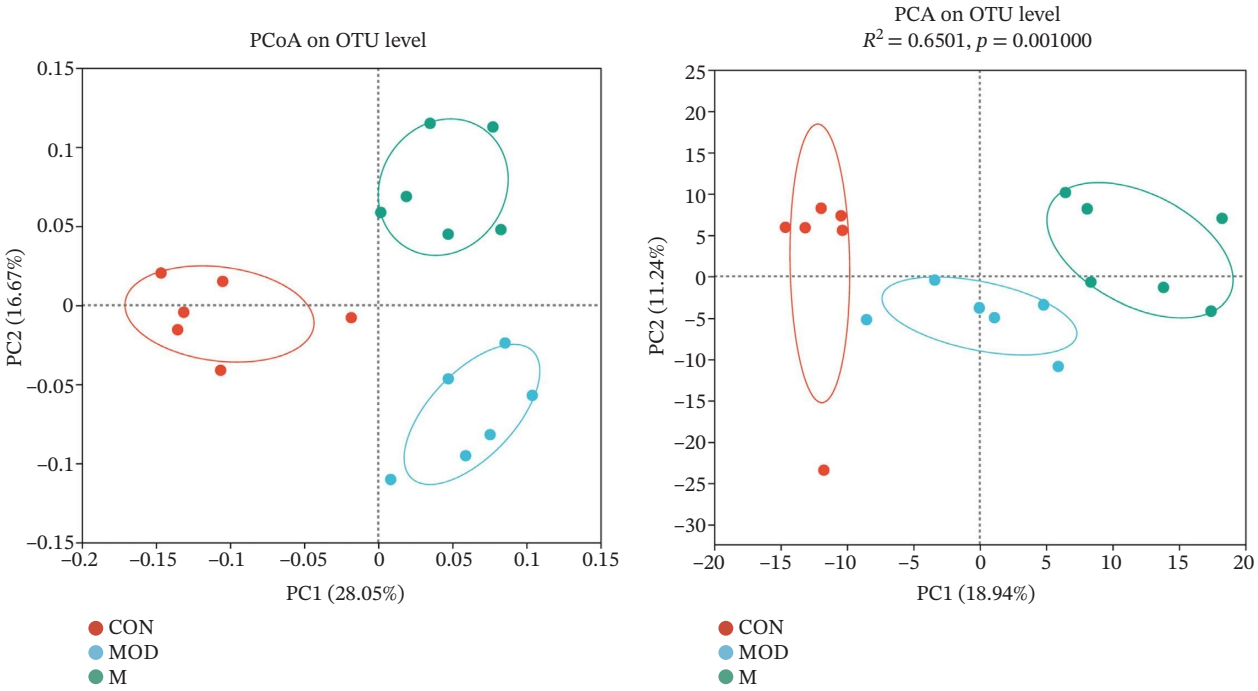

FIGURE 7 | FPP-1-1 (100 mg/kg) treatment increases gut microbiota beta diversity ($n = 6$).

The main microbial biomarkers among the groups were determined by the linear discriminant analysis (LDA) effect size (LEfSe), and the greater the LDA score, the greater the influence of species abundance on the differential effect. Representative species with LDA scores higher than 4 in each group were analyzed (Figure 10). The result showed that the *c_Bacilli*, *p_Firmicutes*, *f_Lactobacillaceae*, *g_Lactobacillus*, and *o_Lactobacillales* were enriched in the control group. However, *o_Bacteroidales*, *c_Bacteroidia*, *p_Bacteroidota*, and *f_Muribaculaceae* exhibited higher relative proportions in the model group. Moreover, *c_Clostridia*, *o_Lachnospirales*, *f_Lachnospiraceae*, and *g_Lachnospiraceae_NK4A136_group* were more abundant in the 100 mg/kg FPP-1-1 group.

3.5.7 | Correlation Analysis Between MAPK/NF-κB Pathway and Inflammatory Cytokines and Gut Microbiota

Next, Spearman's analysis was applied to explore the relationship between gut microbes and cytokines. As shown in Figure 11(a), the IL-10 was positively associated with *p_Firmicutes*, *g_Lactobacillus*, and negatively associated with *g_Dubosiella*,

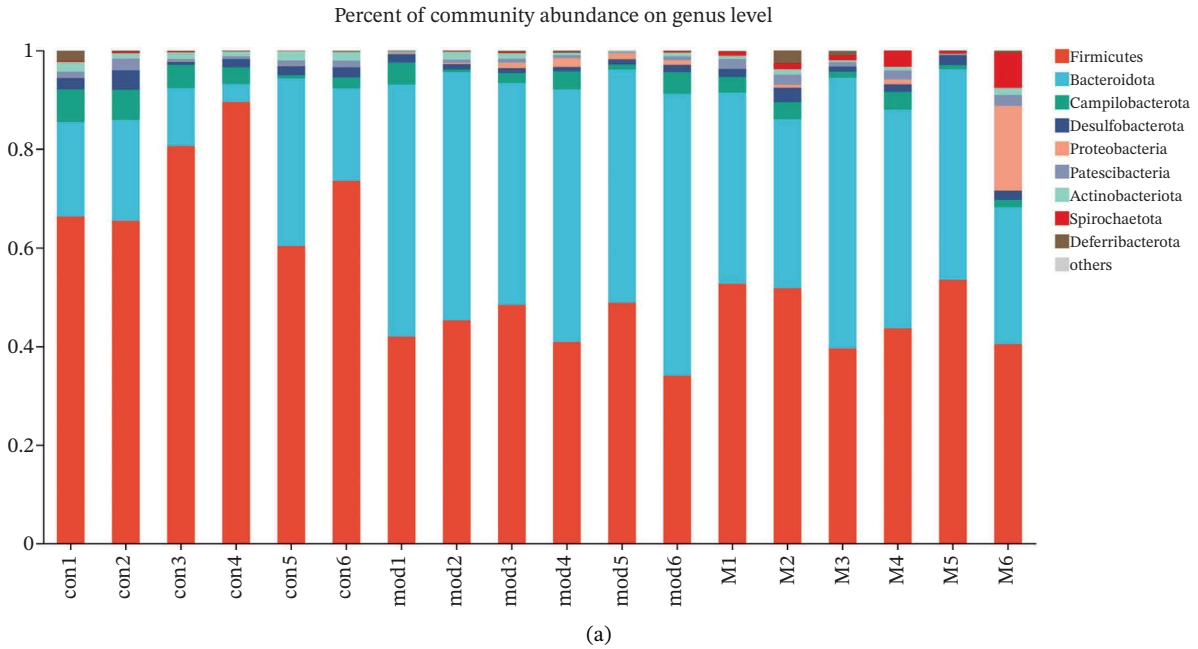

(a)

FIGURE 8 | (Continued)

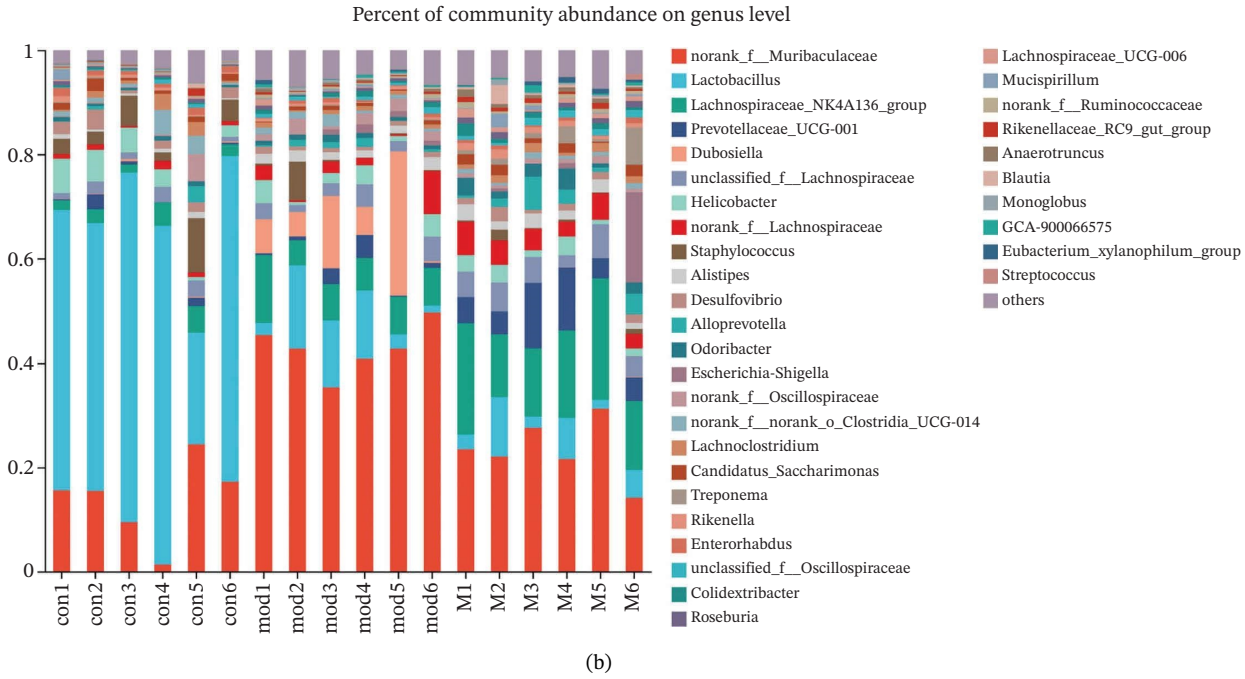

(b)

FIGURE 8 | FPP-1-1 (100 mg/kg) treatment modulates the microbial community structure in the mice with LPS-induced ALI. (a) Analysis of community barplot abundance at the phylum level. (b) Analysis of community barplot abundance at the genus level ($n = 6$).

g_Lachnospiraceae_NK4A136_group, *p_Bacteroidota*, *g_norank_f_Muribaculaceae*. IL-6, TNF-α, *p*-ERK and p-p65 were positively associated with *g_Dubosiella*, *g_unclassified_f_Lachnospiraceae*, *g_Lachnospiraceae_NK4A136_group*, and p-p65 is positively associated with *p_Proteobacteria*, *g__Escherichia.Shigella*, *g_Dubosiella*, *g_Odoribacter*, and negatively associated with *p_Firmicutes*, *g_Lactobacillus* in the control and model groups. As shown in Figure 11(b), IL-10 was positively associated with *g_Prevotellaceae_UCG.001*, *g_Alloprevotella*, and negatively associated with *g_Dubosiella*. IL-6, TNF-α, *p*-ERK and p-p65 were positively associated with *g_norank_f_Muribaculaceae* and *g_Dubosiella* and negatively associated with *p_Spirochaetota*, *g_Treponema*, *g_Candidatus_Saccharimonas*, *g_Prevotellaceae_UCG.001*, and *g_Alloprevotella* in the model and FPP-1-1 (100 mg/kg) treatment groups.

4 | Discussion

The structural characteristics of polysaccharides are closely associated with their biological activity, and elucidation of their structure can help reveal their pharmacological activity [29]. In this study, crude polysaccharides from *F. pumila* were purified using a DEAE-52 column and Sephadex G-100 column to obtain FPP-1-1. The total carbohydrate, protein, and uronic acid contents in FPP-1-1 were determined to be 98.4%, 0.86%, and 25.14%, respectively, using the corresponding methods. These results indicated that FPP-1-1 is an acidic polysaccharide. UV–Vis and IR are commonly used techniques for analyzing the functional groups of polysaccharides for structural elucidation [30]. In this study, FPP-1-1 was measured using UV–Vis and FTIR spectroscopy, and the polysaccharide structure of FPP-1-1 was determined. The polysaccharide did not absorb any proteins, according to the UV–Vis data, and the IR spectrum had typical hydroxyl and carbonyl absorption peaks. The results were the same as those of the compositional analysis. Polysaccharide structure analysis depends on the Mw and monosaccharide groups of polysaccharides. The HPGPC method was used to evaluate the relative molecular mass of FPP-1-1 by comparing its retention time with that of dextran of standard Mw [31]. Using this method, the relative Mw of FPP-1-1 was 1.29×10^6 Da. FPP-1-1 contains Rha, Man, GlcUA, Glc, GalUA, Gal, Ara, and Fuc in a ratio of 5.55:1.79: 1.05:3.67: 1.00:49.52: 13.43:1.10 through PMP precolumn derivatization and HPLC.

ALI is an acute lung disease with a high mortality rate; inflammation plays critical roles in the etiology of ALI [32]. LPS is a bacterial endotoxin, and its intraperitoneal injection can mimic more severe clinical stages, which is widely used to simulate the early manifestations of ALI [33]. Pulmonary edema, widespread inflammatory cell infiltration, and alveolar shrinkage are characteristic features of LPS-induced ALI. In this study, we performed H&E staining and determined the lung tissue W/D ratio to determine whether the LPS-induced ALI mouse model was successfully established. The results showed that ALI was successfully induced after intraperitoneal LPS injection, and these symptoms were greatly relieved after FPP-1-1 treatment (50 mg/kg, 100 mg/kg, and 200 mg/kg).

TNF-α and IL-6 are key inflammatory factors that induce lung injury and are also early markers of ALI. During the onset of ALI, the activation of the MAPK/NF-κB pathway induces the production and release of TNF-α and IL-6 by inflammatory cells, further promoting the migration of neutrophils to the interstitial tissue and lung infiltration, which leads to a severe inflammatory response [34, 35]. In the LPS-induced mouse model of ALI, the expression levels of TNF-α and IL-6 were positively correlated with the severity of lung tissue damage. IL-10 acts as a pivotal anti-inflammatory regulator, attenuating excessive inflammation by inhibiting the MAPK/NF-κB signaling pathways, which

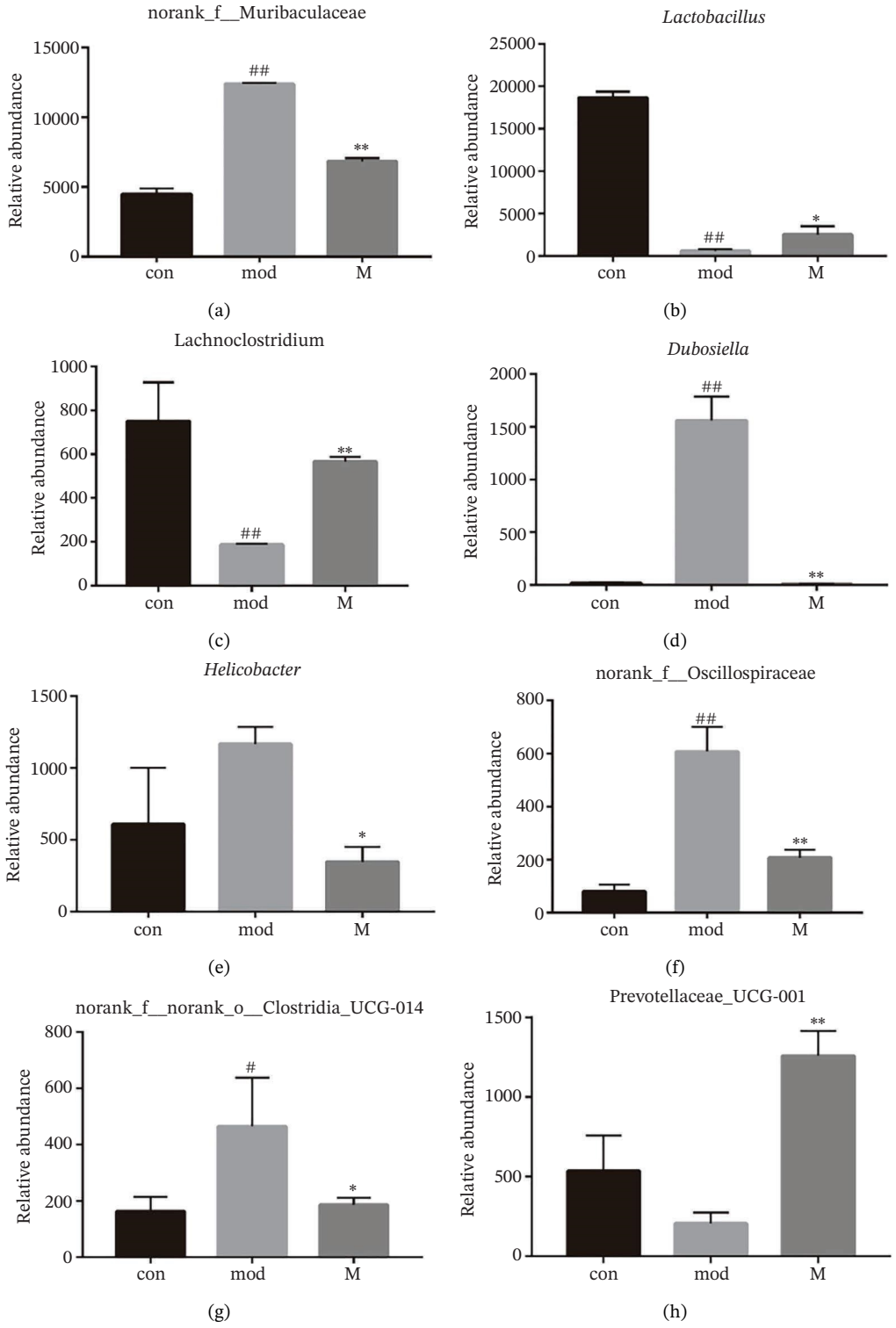

FIGURE 9 | The relative proportion of the main gut microbiota at the genus level ($n = 6$). $^{\#\#}p < 0.01$ compared to the control group, $^{**}p < 0.01$ compared to the model group.

subsequently reduces the secretion of proinflammatory cytokines, such as TNF-α and IL-6 [36, 37]. IL-10 has been shown to exert a protective effect against LPS-induced ALI [38]. In this study, TNF-α and IL-6 levels increased after LPS injection, but IL-10 levels decreased in BALF. Following FPP-1-1 treatment, the levels of TNF-α and IL-6 were considerably decreased, while IL-10 levels were increased. The corresponding mRNA expression of TNF-α and IL-6 also increased, and IL-10 mRNA expression was lowered. This suggests that FPP-1-1 alleviates ALI by inhibiting the proinflammatory factors TNF-α and IL-6 and promoting the anti-inflammatory factor IL-10 secretion.

The MAPK family primarily includes p38 MAPK and ERK, with ERK involved in cellular responses triggered by bacterial

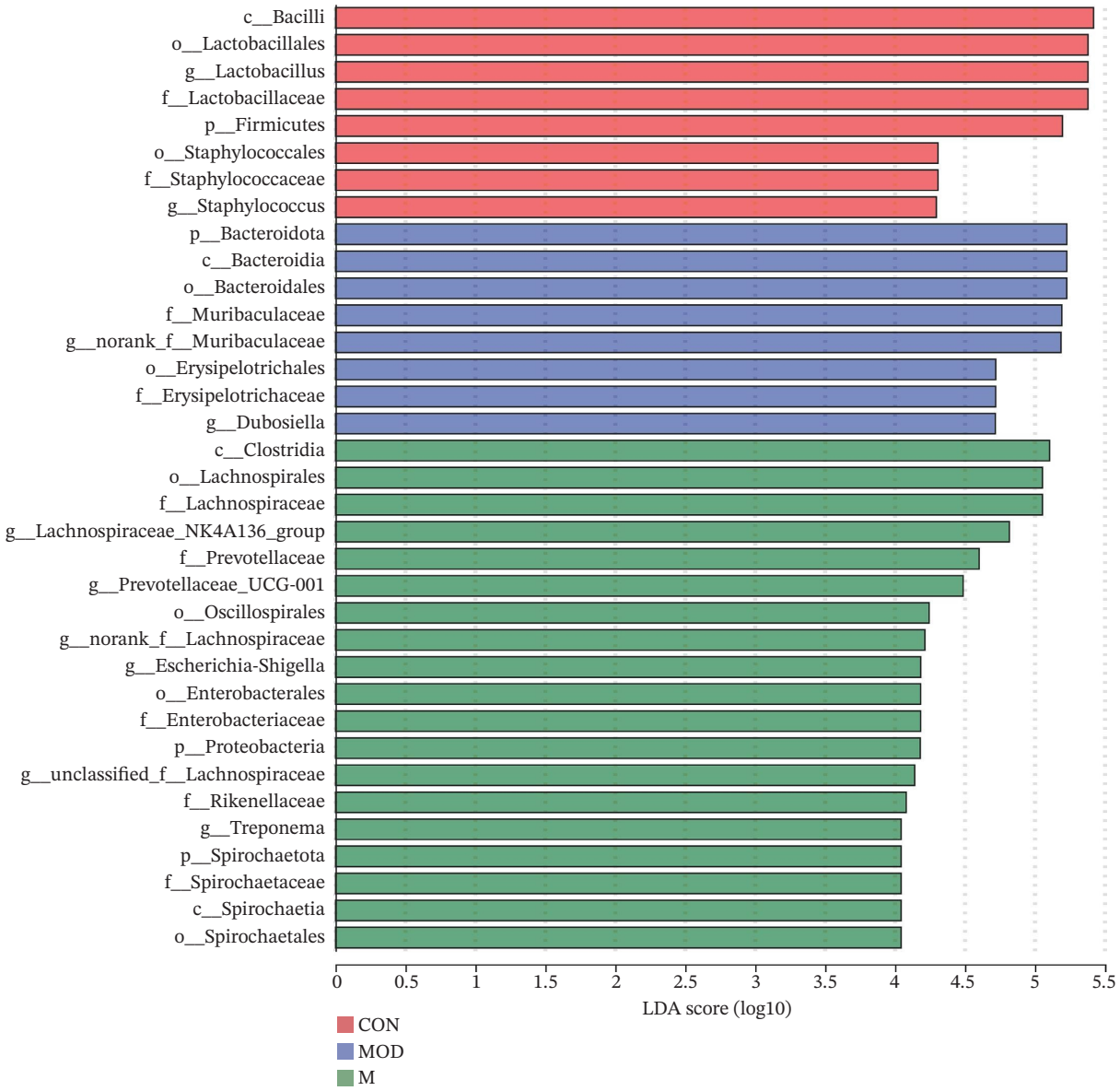

FIGURE 10 | Linear discriminant analysis (LDA) effect size (LEfSe) of dominant flora in the gut ($n = 6$).

products and inflammatory mediators. The function of p38 protein is closely associated with inflammation, apoptosis, and growth [39, 40]. Studies have demonstrated that inhibiting the phosphorylation of p38 MAPK and ERK proteins suppresses the excessive expression of inflammatory factors IL-6 and TNF-α induced by LPS, thereby reducing lung tissue permeability and alleviating ALI [41]. NF-κB is a key downstream target of the MAPK signaling pathway, as the MAPK cascade further activates NF-κB. Upon activation, the NF-κB p65 complex translocates from the cytoplasm to the nucleus, where it binds to the promoter regions of genes encoding proinflammatory mediators (e.g., TNF-α, IL-6) and triggers their transcription, thereby inducing inflammatory responses [42]. Inhibition of NF-κB activation can reduce the production of proinflammatory mediators, thereby mitigating ALI [43, 44]. Inhibition of MAPK/NF-κB pathway expression has been demonstrated to ameliorate ALI [10, 45]. After LPS stimulation, the levels of phosphorylated p38, ERK1/2, and NF-κB p65 increased in the model group, whereas the expression of these three proteins decreased significantly in the FPP-1-1 treatment group. These findings indicate that FPP-1-1 alleviates ALI, possibly by inhibiting the activity of the MAPK/NF-κB pathways.

ALI can stimulate an inflammatory response in the body, which subsequently impairs the intestinal barrier integrity and thereby affects the abundance and diversity [46]. In turn, reduced gut microbiota abundance and diversity may further worsen ALI [47]. In our study, gut microbiota abundance was significantly reduced in mice with LPS-induced inflammation, consistent with previous reports [48]. FPP-1-1 (100 mg/kg) treatment significantly increased the gut microbiota diversity and abundance. Furthermore, FPP-1-1 decreased the abundance of *norrank_f_Oscillosporaceae, Dubosiella*, and *Helicobacter* and increased the abundance of *Lactobacillus*, *Lachnoclostridium*, and *Prevotellaceae_UCG-001*. *Helicobacter* infection promotes the secretion of IL-8 and IL-6 through exotoxin-mediated activation of NF-κB signaling, leading to lung injury [49]. *Lactobacillus* is widely used as an important probiotic that helps protect the

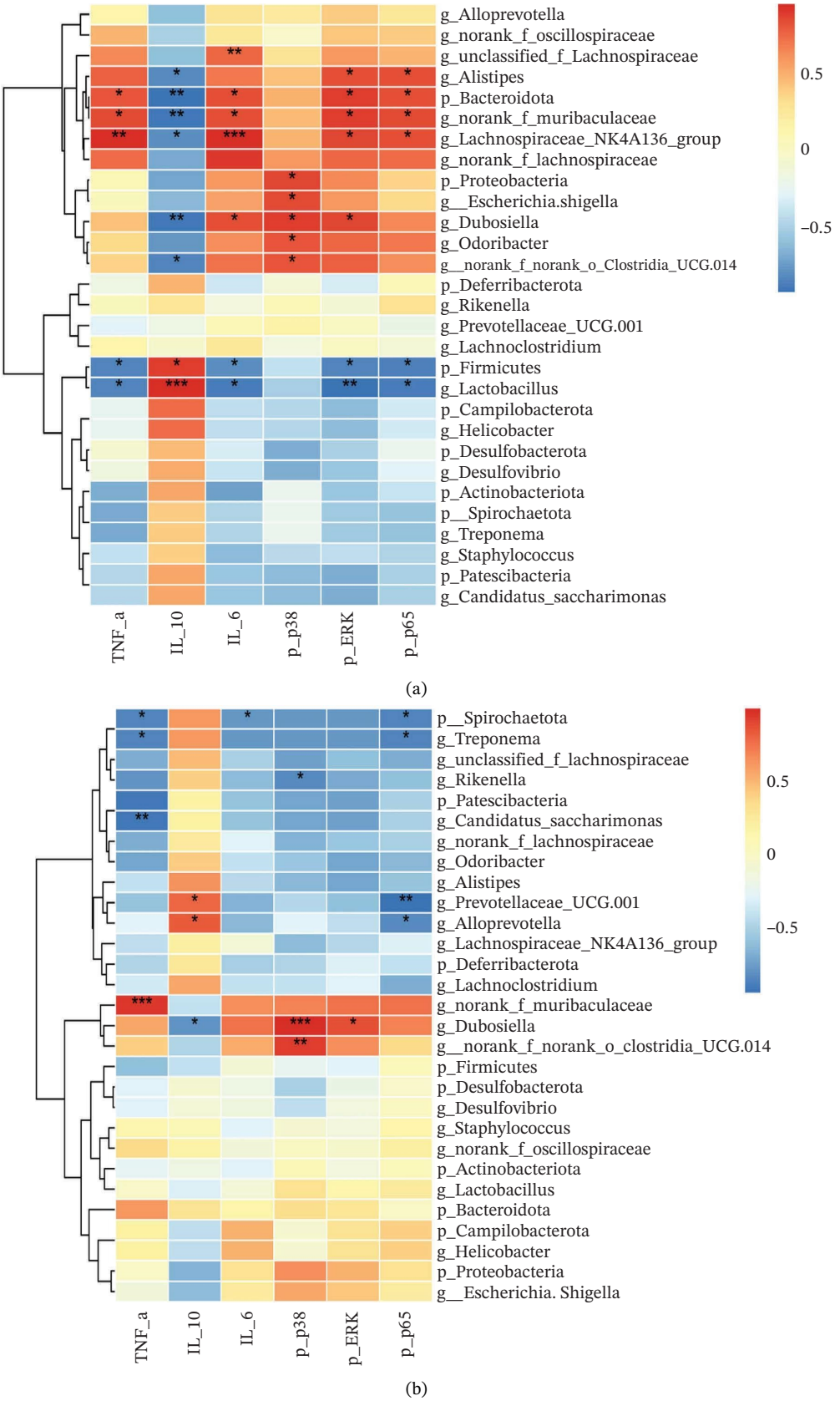

FIGURE 11 | Correlation between gut microbiota and the MAPK/NF-κB pathway and inflammatory cytokines ($n = 6$). (a) Heat maps of correlation between gut microbiota and the MAPK/NF-κB pathway and inflammatory cytokines in control and model groups. (b) Heat maps of correlation between gut microbiota and the MAPK/NF-κB pathway and inflammatory cytokines in model and 100 mg/kg FPP-1-1 groups. Blue indicates a negative correlation, red indicates a positive correlation, and the darker the color, the stronger the correlation. $^{*}p < 0.05$, $^{**}p < 0.01$, $^{***}p < 0.001$.

intestinal mucosal barrier, and *Lactobacillus reuteri* can repair the damaged gut barrier and remodel the microbiota, thereby reducing the inflammatory response [50]. LEfSe results showed that the relative abundances of proinflammatory bacteria *o_Bacteroidales*, *c_Bacteroidia*, and *p_Bacteroidota* were higher in the model group. However, the relative abundances of anti-inflammatory bacteria *o_Lachnospirales* and *f_Lachnospiraceae* were more abundant in the FPP-1-1 100 mg/kg group. *Lachnospiraceae* is a highly abundant member of the gut bacteria able to synthesize SCFAs by fermenting dietary polysaccharides; increasing the abundance of *Lachnospiraceae* can reduce inflammation by enhancing the gut barrier and inhibiting the transfer of LPS [51]. Further studies are needed to determine whether *Lachnospiraceae* plays a key role in the treatment of ALI.

Correlation analysis results showed that *p_Firmicutes*, *g_Lactobacillus*, *g_Prevotellaceae_UCG.001* were significantly correlated with cytokines TNF-α, IL-6, and IL-10, suggesting that *p_Firmicutes*, *g_Lactobacillus,* and *g_Prevotellaceae_UCG.001* may play an anti-inflammatory role in AIL. In addition, *g_Alloprevotella* is negatively associated with p-p65. Both *Alloprevotella* and *Lachnospiraceae* produce butyrate during metabolic processes. Sodium butyrate ameliorated inflammation of COPD induced by cigarette smoke through inhibiting NF-κB/MAPK signaling pathways [52, 53]. Overall, our study suggests that FPP-1-1 (100 mg/kg) alleviates LPS-induced ALI, probably through regulating gut microbiota and then inhibiting the NF-κB/MAPK pathway via the "gut–lung" axis.

5 | Conclusions

The present study characterized the structure and Mw of a novel homogeneous polysaccharide, FPP-1-1, isolated from *F. pumila* and identified its eight branched chain monosaccharides: Rha, Man, GlcUA, Glc, GalUA, Gal, Ara, and Fuc. In vivo experiments demonstrated that FPP-1-1 (50 mg/kg, 100 mg/kg, and 200 mg/kg) significantly inhibited the production of proinflammatory factors TNF-α and IL-6 and increased the production of anti-inflammatory factor IL-10 to alleviate ALI, the mechanism of which is related to the NF-κB/MAPK pathway. Moreover, we showed that FPP-1-1 (100 mg/kg) significantly increased the diversity of gut microbiota in ALI mice and changed the relative abundance of key bacterial genera such as *Lachnospiraceae* and *Alloprevotella*, suggesting that the "gut–lung" axis may be an important pathway for the action of FPP-1-1. However, this study has certain limitations: The dose- and time-dependent effects of LPS stimulation remain unclear, and pathway-specific inhibitors or gene knockout models have not been employed to dissect the independent contributions of individual signaling pathways. Future research will focus on the following aspects: systematically analyzing the dose-dependent and time-dependent effects of LPS stimulation to further evaluate the functional potential of FPP-1-1; utilizing specific pathway inhibitors and gene knockout models to dissect the independent contributions of the ERK, p38, and NF-κB subpathways to the protective effects of FPP-1-1, thereby identifying the core signaling molecules targeted by FPP-1-1.

Author Contributions

Shiying Mai and Liyan Li: data curation, methodology, visualization, writing–original draft; Yinfeng Tan, Minghai Fu, and Fang Zhang: methodology, data curation, investigation; Junqing Zhang and Yonghui Li: conceptualization, data curation, project administration; Yuhuang Wu and Qi Wang: conceptualization, methodology, writing–review and editing.

Funding

This work was supported by the Major Science and Technology Projects of the Hainan Province (no. ZDKJ202003); Hainan Natural Science Foundation (no. 820RC768); National Natural Science Foundation of China (no. 82160826).

Disclosure

All authors have read and approved the final manuscript for publication.

Conflicts of Interest

The authors declare no conflicts of interest.

Data Availability Statement

Data will be made available on request.

References

1. A. J. Sweatt and J. E. Levitt, "Evolving Epidemiology and Definitions of the Acute Respiratory Distress Syndrome and Early Acute Lung Injury," *Clinics in Chest Medicine* 35, no. 4 (2014): 609–624, https://doi.org/10.1016/j.ccm.2014.08.002.

2. D. Mokra and P. Kosutova, "Biomarkers in Acute Lung Injury," *Respiratory Physiology & Neurobiology* 209 (2015): 52–58, https://doi.org/10.1016/j.resp.2014.10.006.

3. L. J. Cross and M. A. Matthay, "Biomarkers in Acute Lung Injury: Insights Into the Pathogenesis of Acute Lung Injury," *Critical Care Clinics* 27, no. 2 (2011): 355–377, https://doi.org/10.1016/j.ccc.2010.12.005.

4. E. R. Johnson and M. A. Matthay, "Acute Lung Injury Epidemiology: Pathogenesis, and Treatment," *Journal of Aerosol Medicine and Pulmonary Drug Delivery* 23, no. 4 (2010): 243–252, https://doi.org/10.1089/jamp.2009.0775.

5. F. Michard, F. M. Enrique, M. Y. Kirov, Malbrain, and T. Tagami, "A New and Simple Definition for Acute Lung Injury," *Critical Care Medicine* 40, no. 3 (2012): 1004–1006, https://doi.org/10.1097/CCM.0b013e31823b97fd.

6. A. T. Dang and B. J. Marsland, "Microbes, Metabolites, and the Gut-Lung Axis," *Mucosal Immunology* 12, no. 4 (2019): 843–850, https://doi.org/10.1038/s41385-019-0160-6.

7. J. J. Wu, Y. B. Xu, B. Zhu, et al., "Characterization of an Arabinogalactan From the Fruit Hulls of *Ficus Pumila* Linn. and Its Immunomodulatory Effect," *Journal of Functional Foods* 73 (2020): 104091, https://doi.org/10.1016/j.jff.2020.104091.

8. Z. Y. Qi, J. Y. Zhao, F. J. Lin, W. L. Zhou, and R. Y. Gan, "Bioactive Compounds, Therapeutic Activities, and Applications of *Ficus Pumila L.*," *Agronomy* 11, no. 1 (2021): 89, https://doi.org/10.3390/agronomy11010089.

9. K. Suzuki, K. Gonda, Y. Kishimoto, Y. Katsumoto, and S. Takenoshita, "Potential Curing and Beneficial Effects of Ooitabi (Ficus Pumila L.) on Hypertension and Dyslipidaemia in Okinawa," *Journal of Human Nutrition and Dietetics* 34, no. 2 (2021): 395–401, https://doi.org/10.1111/jhn.12806.

10. J. Chen, X. Xue, J. Q. Cai, L. Jia, B. D. Sun, and W. Zhao, "Protective Effect of Taurine on Sepsisinduced Lung Injury via Inhibiting the p38/MAPK Signaling Pathway," *Molecular Medicine Reports* 24, no. 3 (2021): 653, https://doi.org/10.3892/mmr.2021.12292.

11. X. Yang, A. Q. Li, X. X. Li, L. J. Sun, and Y. R. Guo, "An Overview of Classifications, Properties of Food Polysaccharides and Their Links to

Applications in Improving Food Textures," *Trends in Food Science and Technology* 102 (2020): 1–15, https://doi.org/10.1016/j.tifs.2020.05.020.

12. C. Y. Hou, L. L. Chen, L. Z. Yang, and X. L. Ji, "An Insight Into Anti-Inflammatory Effects of Natural Polysaccharides," *International Journal of Biological Macromolecules* 153 (2020): 248–255, https://doi.org/10.1016/j.ijbiomac.2020.02.315.

13. L. Chen and G. L. Huang, "Antitumor Activity of Polysaccharides: An Overview," *Current Drug Targets* 19, no. 1 (2018): 89–96, https://doi.org/10.2174/1389450118666170704143018.

14. M. Yin, Y. Zhang, and H. Li, "Advances in Research on Immunoregulation of Macrophages by Plant Polysaccharides," *Frontiers in Immunology* 10 (2019): 145, https://doi.org/10.3389/fimmu.2019.00145.

15. J. Liu, Y. P. Zhao, Q. X. Wu, et al., "Structure Characterisation of Polysaccharides in Vegetable "Okra" and Evaluation of Hypoglycemic Activity," *Food Chemistry* 242 (2018): 211–216, https://doi.org/10.1016/j.foodchem.2017.09.051.

16. L. Chen and G. L. Huang, "The Antiviral Activity of Polysaccharides and Their Derivatives," *International Journal of Biological Macromolecules* 115 (2018): 77–82, https://doi.org/10.1016/j.ijbiomac.2018.04.056.

17. M. M. Bradford, "A Rapid and Sensitive Method for the Quantitation of Microgram Quantities of Protein Utilizing the Principle of Protein-Dye Binding," *Analytical Biochemistry* 72, no. 1-2 (1976): 248–254, https://doi.org/10.1006/abio.1976.9999.

18. S. K. Saha and C. F. Brewer, "Determination of the Concentrations of Oligosaccharides, Complex Type Carbohydrates, and Glycoproteins Using the Phenol-Sulfuric Acid Method," *Carbohydrate Research* 254 (1994): 157–167, https://doi.org/10.1016/0008-6215(94)84249-3.

19. Y. Liu, Y. Y. Sun, and G. L. Huang, "Preparation and Antioxidant Activities of Important Traditional Plant Polysaccharides," *International Journal of Biological Macromolecules* 111 (2018): 780–786, https://doi.org/10.1016/j.ijbiomac.2018.01.086.

20. J. Meng, K. Deng, N. Hu, and H. L. Wang, "Nitraria Tangutorum Bobr-Derived Polysaccharides Protect Against LPS-Induced Lung Injury," *International Journal of Biological Macromolecules* 186 (2021): 71–78, https://doi.org/10.1016/j.ijbiomac.2021.06.181.

21. Y. P. Ren and S. X. Liu, "Effects of Separation and Purification on Structural Characteristics of Polysaccharide From Quinoa (Chenopodium Quinoa Willd)," *Biochemical and Biophysical Research Communications* 522, no. 2 (2020): 286–291, https://doi.org/10.1016/j.bbrc.2019.10.030.

22. H. Zhang, P. Zou, H. T. Zhao, J. Q. Qiu, J. M. Regenstein, and X. Yang, "Isolation, Purification, Structure and Antioxidant Activity of Polysaccharide From Pinecones of Pinus Koraiensis," *Carbohydrate Polymers* 251 (2021): 117078, https://doi.org/10.1016/j.carbpol.2020.117078.

23. Z. Wu, W. Z. Zeng, X. Zhang, and J. F. Yang, "Characterization of Acidic Tea Polysaccharides From Yellow Leaves of Wuyi Rock Tea and Their Hypoglycemic Activity via Intestinal Flora Regulation in Rats," *Foods* 11, no. 4 (2022): 617, https://doi.org/10.3390/foods11040617.

24. Y. F. Wang, X. L. Wei, and Z. Y. Jin, "Structure Analysis of an Acidic Polysaccharide Isolated From Green Tea," *Natural Product Research* 23, no. 7 (2009): 678–687, https://doi.org/10.1080/14786410902819178.

25. M. K. Lu, C. C. Chang, C. H. Chao, and Y. C. Hsu, "Structural Changes, and Anti-Inflammatory, Anti-Cancer Potential of Polysaccharides From Multiple Processing of Rehmannia Glutinosa," *International Journal of Biological Macromolecules* 206 (2022): 621–632, https://doi.org/10.1016/j.ijbiomac.2022.02.112.

26. C. Y. Liu, J. Meng, J. Y. Qiu, X. Q. Geng, H. Q. Sun, and Z. Y. Zhu, "Structural Characterization and Prebiotic Potential of an Acidic Polysaccharide From Imperial Chrysanthemum," *Natural Product Research* 36, no. 2 (2022): 586–594, https://doi.org/10.1080/14786419.2020.1795657.

27. X. Y. Mei, W. J. Yang, G. L. Huang, and H. L. Huang, "The Antioxidant Activities of Balsam Pear Polysaccharide," *International Journal of Biological Macromolecules* 142 (2020): 232–236, https://doi.org/10.1016/j.ijbiomac.2019.09.168.

28. W. J. Yang and G. L. Huang, "Extraction, Structural Characterization, and Physicochemical Properties of Polysaccharide From Purple Sweet Potato," *Chemical Biology & Drug Design* 98, no. 6 (2021): 979–985, https://doi.org/10.1111/cbdd.13952.

29. Y. Xu, Y. J. Wu, P. L. Sun, F. M. Zhang, R. J. Linhardt, and A. Q. Zhang, "Chemically Modified Polysaccharides: Synthesis, Characterization, Structure Activity Relationships of Action," *International Journal of Biological Macromolecules* 132 (2019): 970–977, https://doi.org/10.1016/j.ijbiomac.2019.03.213.

30. S. R. Derkach, N. G. Voron'ko, N. I. Sokolan, D. S. Kolotova, and Y. A. Kuchina, "Interactions Between Gelatin and Sodium Alginate: Uv-Vis and Ftir Studies," *Journal of Dispersion Science and Technology* 41, no. 5 (2019): 690–698, https://doi.org/10.1080/01932691.2019.1611437.

31. J. Xu, S. L. Li, R. Q. Yue, et al., "A Novel and Rapid HpgpC-Based Strategy for Quality Control of Saccharide-Dominant Herbal Materials: Dendrobium Officinale, a Case Study," *Analytical and Bioanalytical Chemistry* 406, no. 25 (2014): 6409–6417, https://doi.org/10.1007/s00216-014-8060-9.

32. K. W. Wang, H. R. Zhang, J. Q. Zhang, E. J. Jia, and G. S. Zhu, "Prediction of Immune Factors and Signaling Pathways in Lung Injury Induced by LPS Based on Network Analysis," *Saudi Journal of Biological Sciences* 26, no. 8 (2019): 2068–2073, https://doi.org/10.1016/j.sjbs.2019.09.014.

33. W. Li, Z. H. Ding, Y. Chen, et al., "Integrated Pharmacology Reveals the Molecular Mechanism of Gegen Qinlian Decoction Against Lipopolysaccharide-Induced Acute Lung Injury," *Frontiers in Pharmacology* 13 (2022): 854544, https://doi.org/10.3389/fphar.2022.854544.

34. T. Q. Xuan, G. H. Gong, H. H. Du, et al., "Protective Effect of Pteryxin on LPS-Induced Acute Lung Injury via Modulating Mapk/NF-*K*B Pathway and Nlrp3 Inflammasome Activation," *Journal of Ethnopharmacology* 286 (2022): 114924, https://doi.org/10.1016/j.jep.2021.114924.

35. X. Z. Han, R. Ma, Q. Chen, et al., "Anti-Inflammatory Action of Athyrium Multidentatum Extract Suppresses the LPS-Induced TLR4 Signaling Pathway," *Journal of Ethnopharmacology* 217 (2018): 220–227, https://doi.org/10.1016/j.jep.2018.02.031.

36. Y. L. Yin, W. W. Liu, G. Ji, and Y. L. Dai, "The Essential Role of p38 Mapk in Mediating the Interplay of Oxldl and IL-10 in Regulating Endothelial Cell Apoptosis," *European Journal of Cell Biology* 92, no. 4-5 (2013): 150–159, https://doi.org/10.1016/j.ejcb.2013.01.001.

37. B. Mishra, R. Yuan, C. Wingert, et al., "IL-10 Targets IRF Transcription Factors to Suppress IFN and Inflammatory Response Genes by Epigenetic Mechanisms," *Nature Immunology* 26, no. 5 (2025): 748–759, https://doi.org/10.1038/s41590-025-02137-3.

38. Z. Sun, A. M. Chen, M. Huang, et al., "B Cell-Derived IL-10 Promotes the Resolution of Lipopolysaccharide-Induced Acute Lung Injury," *Cell Death & Disease* 14, no. 7 (2023): 418, https://doi.org/10.1038/s41419-023-05954-2.

39. R. Li, Y. Ma, H. R. Wu, et al., "4-Octyl Itaconate Alleviates Endothelial Cell Inflammation and Barrier Dysfunction in LPS-Induced Sepsis via Modulating TLR4/MAPK/NF-*K*B Signaling: 4-Octyl Itaconate Alleviates Endothelial Dysfunction," *Molecular Medicine* 31, no. 1 (2025): 240, https://doi.org/10.1186/s10020-025-01160-2.

40. T. Farkhondeh, O. Mehrpour, C. Buhrmann, A. M. Pourbagher-Shahri, M. Shakibaei, and S. Samarghandian, "Organophosphorus Compounds and Mapk Signaling Pathways," *International Journal of Molecular Sciences* 21, no. 12 (2020): 4258, https://doi.org/10.3390/ijms21124258.

41. H. W. Hong, S. Y. Lou, F. L. Zheng, et al., "Hydnocarpin D Attenuates Lipopolysaccharide-Induced Acute Lung Injury via Mapk/NF-*K*B and Keap1/Nrf2/HO-1 Pathway," *Phytomedicine* 101 (2022): 154143, https://doi.org/10.1016/j.phymed.2022.154143.

42. C. L. Tian, P. Zhang, J. Yang, et al., "The Protective Effect of the Flavonoid Fraction of Abutilon Theophrasti Medic. Leaves on LPS-Induced Acute Lung Injury in Mice via the NF-*K*B and Mapk Signalling Pathways," *Biomedicine & Pharmacotherapy* 109 (2019): 1024–1031, https://doi.org/10.1016/j.biopha.2018.10.197.

43. Y. H. Zhai, K. J. Chen, Z. C. Xu, et al., "Harmine Alleviates LPS-Induced Acute Lung Injury by Inhibiting CSF3-Mediated Mapk/NF-*K*B Signaling Pathway," *Respiratory Research* 26, no. 1 (2025): 119, https://doi.org/10.1186/s12931-025-03196-8.

44. Y. X. Wu, Y. J. Nie, J. F. Huang, et al., "Protostemonine Alleviates Heat-Killed Methicillin-Resistant Staphylococcus Aureus-Induced Acute Lung Injury Through Mapk and NF-*K*B Signaling Pathways," *International Immunopharmacology* 77 (2019): 105964, https://doi.org/10.1016/j.intimp.2019.105964.

45. M. Zhou, L. Meng, Q. K. He, C. G. Ren, and C. Y. Li, "Valsartan Attenuates LPS-Induced ALI by Modulating NF-*K*B and Mapk Pathways," *Frontiers in Pharmacology* 15 (2024): 1321095, https://doi.org/10.3389/fphar.2024.1321095.

46. T. Y. Tang, F. Wang, J. Liu, W. Ye, T. Zhao, and Z. J. Li, "Rhubarb Alleviates Acute Lung Injury by Modulating Gut Microbiota Dysbiosis in Mice," *Current Microbiology* 79, no. 4 (2022): 116, https://doi.org/10.1007/s00284-022-02811-X.

47. J. Tang, L. Xu, Y. Zeng, and F. Gong, "Effect of Gut Microbiota on LPS-Induced Acute Lung Injury by Regulating the TLR4/NF-KB Signaling Pathway," *International Immunopharmacology* 91 (2021): 107272, https://doi.org/10.1016/j.intimp.2020.107272.

48. D. N. Wei, P. Ma, Q. Q. Fan, H. C. Yu, Yi. Peng, and X. B. Li, "Yanning Syrup Ameliorates the Lipopolysaccharide-Induced Inflammation: Adjusting the Gut Microbiota, Short-Chain Fatty Acids, and the CD4 T Cell Balance," *Journal of Ethnopharmacology* 283 (2022): 114729, https://doi.org/10.1016/j.jep.2021.114729.

49. M. Z. Chen, X. P. Huang, M. Z. Gao, et al., "*Helicobacter Pylori* Promotes Inflammatory Factor Secretion and Lung Injury Through Vaca Exotoxin-Mediated Activation of NF-*K*B Signaling," *Bioengineered* 13, no. 5 (2022): 12760–12771, https://doi.org/10.1080/21655979.2022.2071011.

50. J. Shen, S. T. Wang, Y. Huang, et al., "Lactobacillus Reuteri Ameliorates Lipopolysaccharide-Induced Acute Lung Injury by Modulating the Gut Microbiota in Mice," *Nutrients* 15, no. 19 (2023): 4256, https://doi.org/10.3390/nu15194256.

51. S. B. Huang, J. Z. Chen, Z. J. Cui, et al., "Lachnospiraceae-Derived Butyrate Mediates Protection of High Fermentable Fiber Against Placental Inflammation in Gestational Diabetes Mellitus," *Science Advances* 9, no. 44 (2023): 7337, https://doi.org/10.1126/sciadv.adi7337.

52. Y. Yuan, L. Li, B. Nan, C. Y. Yang, and H. Y. Yan, "Allicin Ameliorates Intestinal Barrier Damage via Microbiota-Regulated Short-Chain Fatty Acids-TLR4/MyD88/NF-*K*B Cascade Response in Acrylamide-Induced Rats," *Journal of Agricultural and Food Chemistry* 69, no. 43 (2021): 12837–12852, https://doi.org/10.1021/acs.jafc.1c05014.

53. Z. J. Zhao, Y. Q. Tong, Y. T. Kang, et al., "Sodium Butyrate (SB) Ameliorated Inflammation of Copd Induced by Cigarette Smoke Through Activating the GPR43 to Inhibit NF-*K*B/MAPKs Signaling Pathways," *Molecular Immunology* 163 (2023): 224–234, https://doi.org/10.1016/j.molimm.2023.10.007.